Journal of Neurochemistry

JOURNAL OF NEUROCHEMISTRY | 2015 | 135 | 908–917 doi: 10.1111/jnc.13370

ORIGINAL ARTICLE

Specific binding of [^{18}F]fluoroethyl-harmol to monoamine oxidase A in rat brain cryostat sections, and compartmental analysis of binding in living brain

Simone Maschauer,* Adelina Haller,* Patrick J. Riss,† Torsten Kuwert,* Olaf Prante* and Paul Cumming‡,§

*Laboratory of Molecular Imaging and Radiochemistry, Department of Nuclear Medicine, Friedrich Alexander University, Erlangen, Germany

†Department of Chemistry, Universitetet i Oslo & Norsk Medisinisk Syklotronsenter AS, Oslo, Norway

‡Department of Neuroscience and Pharmacology, Copenhagen University, Copenhagen, Denmark

§Department of Neuropsychiatry and Psychosomatic Medicine, OUS-Rikshospitalet, Oslo, Norway

Abstract

We investigated [^{18}F]fluoroethyl-harmol ([^{18}F]FEH) as a reversible and selective ligand for positron emission tomography (PET) studies of monoamine oxidase A (MAO-A). Binding of [^{18}F]FEH in rat brain cryostat sections indicated high affinity (K_D = 3 nM), and density (B_{max}; 600 pmol/g). The plasma free fraction was 45%, and untransformed parent constituted only 13% of plasma radioactivity at 10 min after injection. Compartmental analysis of PET recordings in pargyline-treated rats showed high permeability to brain (K_1; 0.32 mL/g/min) and slow washout (k_2; 0.024/min), resulting in a uniformly high equilibrium distribution volume (V_D; 20 mL/g). Using this V_D to estimate unbound ligand in brain of untreated rats, the binding potential ranged from 4.2 in cerebellum to 7.2 in thalamus. We also calculated maps of rats receiving [^{18}F]FEH at a range of specific activities, and then estimated saturation binding parameters in the living brain. In thalamus, striatum and frontal cortex K_D was globally close to 300 nM and B_{max} was close to 1600 pmol/g; the 100-fold discrepancy in affinity suggests a very low free fraction for [^{18}F]FEH in the living brain. Based on a synthesis of findings, we calculate the endogenous dopamine concentration to be 0.4 μM in the striatal compartment containing MAO-A, thus unlikely to exert competition against [^{18}F]FEH binding *in vivo*. In summary, [^{18}F]FEH has good properties for the detection of MAO-A in the rat brain by PET, and may present logistic advantages for clinical research at centers lacking a medical cyclotron.

Keywords: fluorine-18, fluoroethyl-harmol, MAO-A, PET. β-carbolines.

J. Neurochem. (2015) **135**, 908–917.

Monoamine oxidase A (MAO-A) is an important target for brain molecular imaging studies, given its key role in the inactivation of biogenic amine neurotransmitters, including serotonin and (along with MAO-B) also dopamine. *In situ* hybridization studies show highest expression of mRNA encoding MAO-A in the locus coeruleus and other adrenergic neurons of the medulla, and in the mesencephalic dopamine and serotonin neurons, whereas MAO-B expression is more diffuse (Jahng *et al.* 1997). Harmine and others β-carbolines are natural product competitive inhibitors of MAO-A, which is the pharmacological basis of their potentiation of the hallucinogenic effect of *N*,*N*-dimethyltryptamine in the ayahuasca ritual (McKenna *et al.* 1984). The radiopharmaceutical [^{11}C]harmine was developed as a ligand for positron emission tomography (PET) studies of MAO-A in the brain and other tissues, based initially upon its

Received June 21, 2015; revised manuscript received September 8, 2015; accepted September 10, 2015.

Address correspondence and reprint requests to Prof. Dr Olaf Prante, Laboratory of Molecular Imaging and Radiochemistry, Department of Nuclear Medicine, Friedrich Alexander University, Schwabachanlage 6, 91054 Erlangen, Germany. E-mail: olaf.prante@uk-erlangen.de

Abbreviations used: [^{18}F]FEH, [^{18}F]fluoroethyl-harmol; AUC, area under the curve; BP_{ND}, binding potential; MAO-A, monoamine oxidase A; PET, positron emission tomography; TFA, trifluoroacetic acid; VOI, volume of interest.

nM affinity and high selectivity for the enzyme (Bergström *et al.* 1997). Despite this background, there have until recently been relatively few PET studies with MAO-A as molecular target. We have used [11C]harmine-PET to verify blockade of MAO-A in pargyline-treated Göttingen minipigs, toward testing an hypothesis that MAO blockade should potentiate the amphetamine-evoked release of dopamine in striatum (Jensen *et al.* 2006). Clinical PET studies with [11C]harmine show increased uptake in the brain of patients with major depression (Chiuccariello *et al.* 2014), lending some support to a biogenic amine insufficiency model (Gryglewski *et al.* 2014).

[11C]harmine is characterized by a rapid metabolism, such that the fraction of untransformed tracer in plasma falls to 10 percent within 15 min after injection, which can present technical difficulties for quantitative analysis of tracer uptake relative to a vanishing arterial input function. Despite this rapid metabolism, [11C]harmine has a very high retention throughout living brain because of the abundance of specific binding in all brain regions and to its high lipophilicity. A [18F]fluorine-labeled derivative might present logistic advantages related to the 109-min physical half-life by enabling multiple scanning from a single radiosynthesis, distribution to PET centers lacking an on-site cyclotron, and possibly improved quantitation of the arterial input function. Some preliminary reports have indicated that [18F]fluoroethylharmol ([18F]FEH) has good properties for PET imaging based on its high affinity and specificity, and lack of brain-penetrating metabolites (Blom *et al.* 2008; Schieferstein *et al.* 2012, 2015). In our preliminary report of the cerebral binding of [18F]FEH in living rats, the binding potential (BP_{ND}) was approximately 2, calculated relative to the non-specific binding in rats with pargyline pre-treatment (Cumming *et al.* 2015). However, arterial inputs were not available in that study, such that the tracer kinetics could not be calculated, nor was the relationship between [18F]FEH uptake and MAO-A enzyme clearly established. Therefore, we undertook a series of new studies, first to determine the distribution of [18F]FEH binding in rat brain cryostat sections with quantitative autoradiography. In small animal PET studies, we obtained metabolite-corrected arterial input measurements, and used compartmental analysis to calculate the kinetics of the tracer uptake in brain of groups of control and pargyline-treated animals. We also obtained PET recordings with [18F]FEH at a range of specific activities and endeavored to calculate from this data, the saturation binding parameters in living brain.

Methods

Radiosynthesis

Authentic standard of 7-(2-fluoroethoxy)-1-methyl-9H-β-carboline (FEH) was prepared from harmol (Sigma-Aldrich, Taufkirchen, Germany) as described previously (Cumming *et al.* 2015). The PET tracer [18F]FEH was prepared by reacting no-carrier-added [18F] fluoride (300–950 MBq) with 2.5 mg (6 μmol) portions of 3-[(1-methyl-9H-β-carboline-7-yl)oxy]ethyl 4-methylbenzenesulfonate in 400 μL dimethyl sulfoxide, also as reported previously with slight modifications. [18F]FEH was isolated by gradient reversed-phase HPLC (Luna C18(2), 250 × 10 mm, 4 mL/min, 15–25% in 35 min CH_3CN/H_2O (v/v) (0.1% trifluoroacetic acid, TFA). The product fraction (t_R = 29 min) was passed through a C18 cartridge (Sep-Pak, Waters, Eschborn, Germany) and eluted with 1 mL ethanol, which was evaporated to dryness; the product was reformulated in 0.9% saline prior to administration.

Autoradiography *in vitro*

At the conclusion of PET recordings, untreated rats from the high specific activity group (N = 3) were killed by decapitation, while still deeply anesthetized. Brains were rapidly removed and frozen by immersion in n-hexane chilled to −50°C by addition of granular dry ice, and stored at −80°C until use. Horizontal sections 16 μm thick were cut with a cryostat microtome (HM550; Microm, Walldorf, Germany), thaw mounted on glass slides, and stored at −20°C until use. After a pre-incubation in buffer (50 mM Tris-HCl, 1 mM $MgCl_2$, pH 7.4) for 15 min at 22°C, the slides were incubated in buffer containing [18F]FEH with specific activity modified by the addition of authentic standard, so as to obtain the final ligand concentrations of 1, 2, 5, 10, 15, and 20 nM. Some sections were incubated in the presence of harmine (1 μM; Sigma-Aldrich, Taufkirchen, Germany) to block specific binding. After incubation for 45 min at 22°C, incubation medium was decanted and the slides were washed (3 × 5 min) by immersion in buffer at 4°C, followed by a short dip in ice-cold distilled water. Autoradiographic standards were generated by evaporation of aqueous solutions (5 μL) of a range of 18F-solutions of known radiochemical concentration (1–20 nM) on glass slides. After rapid drying, brain sections and autoradiographic standards were exposed to imaging plates (Imaging Plate BAS-IP SR, GE Healthcare, Freiburg, Germany) overnight, and quantified with a high-resolution radioluminography laser scanner (DÜRR Medical HD-CR 35 Bio; Raytest, Straubenhardt, Germany) using the software AIDA Image Analyzer (Raytest, Straubenhardt, Germany). The optical density values were converted to pmol per gram of tissue (wet weight, based on density of 1 g/mL) relative to the standards, with subtraction of non-specific binding, which was calculated by linear regression as a function of ligand concentration. The saturation binding parameters B_{max} and K_d were calculated using the software GraphPad Prism (version 5.04; GraphPad Software, La Jolla, CA, USA), assuming a one-site non-linear model.

Acquisition and compartmental analysis of PET data

All rat experiments were performed in accordance with protocols approved by the local animal protection authorities (Government of Central Franconia, Germany, No. 54-2532.2-18/12). Ten male Sprague–Dawley rats (Charles River Laboratories Inc., Sulzfeld, Germany) weighing 220–260 g were used for compartmental analysis; at 90 min prior to the PET experiments five of the animals were pre-treated with pargyline HCl (50 mg/kg, i.p.), which evokes rapid and complete irreversible inhibition of MAO in the rat brain (Cumming *et al.* 1992). Under isoflurane anesthesia, catheters were placed in a femoral vein and artery. After positioning of the animals

in the aperture of the tomograph in a dorsal supine position, [^{18}F]FEH (8–18 MBq; 2–25 MBq/nmol, 0.3–6 nmol per animal) was administered as a slow intravenous bolus injection via the femoral catheter. A series of 150 μL arterial blood samples was collected in heparin-coated vials at 1, 2, 5, 10, 15, 30, and 60 min, whereupon the emission recording concluded. Portions of plasma were obtained by centrifugation (4 min, 2000 *g*), and deproteinated by addition of an equal volume of TFA (10%) and centrifugation (4 min, 20000 *g*). The supernatants (50 μL) were analyzed by reversed-phase HPLC (Chromolith RP-18e, 100 × 4.6 mm, 4 mL/min, 10–100% in 5 min CH_3CN/H_2O (v/v) (0.1% TFA). Fractions were collected at intervals of 0.25 min and ^{18}F-activity was measured in a γ-counter (Wallac Wizard, Perkin-Elmer, Rodgau, Germany). The total plasma radioactivity input function was corrected by fitting the [^{18}F]FEH and ^{18}F-metabolite fractions measured at the six time points to bi-exponential growth and decay functions; knowing the plasma curves for the parent and metabolite, we calculated for each rat the apparent fractional whole body fractional rate constant for tracer metabolism (k_0; per min), and the elimination rate constant for the metabolite pool in plasma (k_{-1}; per min) by linear graphical analysis, as described in detail previously (Cumming *et al.* 1999); this model assumes rapid equilibration of labeled species between the site of metabolism (i.e., liver) and the site of sampling (i.e., plasma). The free fraction in plasma (f_p) was determined by adding [^{18}F]FEH (100 kBq) to plasma samples taken before and after PET scans. Forty μL of portions were transferred to size exclusion chromatography columns (MicroSpin G-50; GE Healthcare, Freiburg, Germany), centrifuged for 2 min at 2000 *g*, and the radioactivities in the filtrate and in the resin were measured in the γ-counter.

The stability of [^{18}F]FEH in rat plasma *in vitro* was determined by adding 5 MBq of radiotracer to rat plasma (200 μL). The mixture was incubated at 37°C, and samples were drawn after 10 min, 30 min, and 3 h. The samples were deproteinated by addition of an equal volume of 10% TFA, centrifuged and the supernatants analyzed by radio-HPLC (Chromolith RP-18e, 100 × 4.6 mm, 4 mL/min, 10–100% in 5 min CH_3CN/H_2O (v/v) (0.1% TFA); t_R = 1.75 min). Additionally, to ascertain the percentage of labeled metabolites in brain tissue, we removed brains from three animals within 10 min of completion of the PET recordings, and homogenized portions of cerebellum in 10 volumes of TFA (10%). After centrifugation, the extracts were analyzed by radio-HPLC as described above.

After induction of anesthesia with isoflurane, a catheter was placed in a tail vein and the animals were positioned in the aperture of the Inveon small animal tomograph (Siemens, Erlangen, Germany). A dynamic emission recording began upon tail vein injection of 8–12 MBq of high specific activity [^{18}F]FEH (corresponding to 0.6–5 nmol/rat) in a volume of 200 μL saline as a slow bolus. Emission recordings consisted of 23 frames, which increased in duration from 10 s to 10 min (12 × 10 s, 3 × 1 min, 5 × 5 min, 3 × 10 min), ending at 60 min post-injection, followed by a 7-min attenuation scan. Image reconstruction was exactly as described previously, and the dynamic sequences were converted to MINC format, summed and registered to an anatomic atlas of the rat brain, also as described previously (la Fougere *et al.* 2010; Cumming *et al.* 2014). Using the programs iFit and Pip (Dr Ole Munk, Aarhus University PET Centre), we calculated voxel-wise parametric maps of the [^{18}F]FEH distribution volumes (mL/g) relative to the individual metabolite-corrected arterial input functions by the method of Logan in the pargyline-blocked condition (V_D-Logan) and in the unblocked condition (V_T-Logan) for each group of (N = 5) rats, where the distribution volumes are defined according to the consensus nomenclature (Innis *et al.* 2007); we also calculated the corresponding distribution volumes in template volumes of interest by a one-tissue compartment (1TC) model (V_D-1TC and V_T-1TC), defined kinetically in terms of apparent unidirectional blood–brain clearance (K_1; mL/g/min), washout rate constant (k_2; per min), and an apparent brain plasma volume (V_p; mL/g). Using the regional group means for V_D-Logan (from voxel-wise maps) and V_D-1TC (for volumes of interest) in the pargyline-treated rats (N = 5), we then calculated BP_{ND} in cerebellum, cortex, striatum, and thalamus of the untreated rats from the corresponding distribution volume ratio (V_T/V_D − 1).

In another PET study in (N = 8) rats, the injected [^{18}F]FEH solution had been modified by addition of cold standard, such that the injected mass of FEH in pairs of rats was 2, 35, 150, and 400 nmol. Using the mean [^{18}F]FEH curve in plasma of control rats (%ID/mL), and the 1TC kinetic results in cerebellum for pargyline-treated rats (K_1 = 0.19 mL/g/min; k_2 = 0.024/min; V_p = 3 mL/g), we calculated a dose scaled common cerebellum curve for unbound tracer in brain. For each specific activity, BP_{ND} maps were then calculated using the method of Zhou *et al.* (2002). We then calculated the saturation binding parameters *in vivo* by Scatchard analysis, in analogy to the method of Farde *et al.* (1986), but using a scaled cerebellum curve as a surrogate for the reference tissue input function. Here, the bound ligand concentration (B) was calculated as the product of regional BP_{ND} and the calculated [^{18}F]FEH concentration in cerebellum at 45–60 min, which was estimated as the product of the injected mass, the %ID/mL in plasma at that time, and the V_D-1TC (20 mL/g) in the pargyline condition, which corresponds to the free ligand concentration in brain (F). Since the data did not afford a stable non-linear fitting of the one-site model, regional saturation binding parameters *in vivo* were estimated by Scatchard analysis (i.e., plotting BP_{ND} as a function B), with averaging of BP_{ND} for the four pairs of rats receiving nearly the same specific activity.

Statistical analysis

All data are presented as mean values ± SD, as specifically described in the figure legends. Significance of effects of pargyline treatment on the [^{18}F]FEH plasma kinetic parameters were assessed by the Student's *t*-test.

Results

The radiosynthesis of [^{18}F]FEH was performed as described before (Cumming *et al.* 2015) with slight modifications of the semi-preparative HPLC separation. With these modifications, the radiotracer could be obtained in high yields of 23–37% (not decay- corrected, referred to [^{18}F]fluoride) and with specific activities of 26–135 GBq/μmol after a total synthesis time of only 50 min. HPLC analysis of the radiotracer incubated in rat plasma revealed no degradation products at 3 h.

To evaluate the distribution of [18F]FEH in the rat brain, we performed quantitative autoradiography studies using cryostat sections of the rat brain. As expected, the radiotracer showed specific binding throughout the rat brain (Fig. 1a and b) with B_{max} values ranging from 337 pmol/g in cerebellum to 806 pmol/g in the thalamus, notably in the habenula (Fig. 1c and d). The K_d was in the range of 2.2–3.4 nM in the brain regions investigated (Table 1).

Size exclusion chromatography of plasma samples collected from rats during PET recordings revealed identical mean plasma free fractions for (N = 3) control (43 ± 6%; range 36–54%) and for (N = 3) pargyline-pretreated rats (43 ± 8%; range 30–55%). Radiochromatographic analysis of brain extracts revealed that 91 ± 1% of recovered radioactivity was untransformed [18F]FEH, whereas the remainder was hydrophilic metabolites eluting with the solvent front.

As depicted in Fig. 2, [18F]FEH was rapidly metabolized in peripheral tissues, such that the parent compound comprised only 11 ± 3% of total plasma activity at 10 min after tracer injection in control animals versus 15 ± 10% in the pargyline-treated group, with the remainder of radioactivity eluting in the solvent front. The mean (± SD) area under the arterial curve for [18F]FEH normalized to percent injected dose (%ID) during 60 min (area under the curve, AUC_{60}) was 1.62 ± 0.61%ID/mL × min in the control group versus 3.84 ± 1.81%ID/mL × min in the pargyline-treated group (p = 0.037) (Fig. 2a); corresponding AUC_{60} values for the 18F-metabolite(s) in plasma were 10.5 ± 0.6 and 34.9 ± 4.7%ID/mL × min ($p < 0.001$) (Fig. 2b). Kinetic analysis of the apparent plasma metabolism indicated a whole-body fractional rate constant for [18F]FEH metabolism (k_0) of 0.185 ± 0.049/min in the control group versus 0.46 ± 0.26/min in the pargyline group (n.s.); corresponding mean rate constants for the elimination of the metabolite pool from plasma (k_{-1}) were 0.0082 ± 0.0028/min and 0.0213 ± 0.0063/min ($p < 0.0005$).

Fitting a 1TC model to the recorded brain time–activity curves (Fig. 3a and b) revealed substantial influx of [18F]FEH from blood to brain; the apparent magnitudes of K_1 were 1.36–1.70 mL/g/min in the control group and 0.25–0.37 mL/g/min in the pargyline-treated group (Table 2).

Table 1 B_{max} and K_d values of different rat brain regions determined by quantitative autoradiography. Values were determined in three independent experiments and given as mean ± standard deviation (SD).

Brain region	B_{max} (pmol/g)	K_d (nM)
Cerebellum	337 ± 51	2.2 ± 1.0
Neocortex	460 ± 42	2.2 ± 0.5
Anterior cingulate cortex	649 ± 45	2.7 ± 0.5
Hippocampus	581 ± 55	2.5 ± 0.4
Striatum	531 ± 61	2.4 ± 0.4
Dorsomedial thalamus	806 ± 100	3.4 ± 0.1

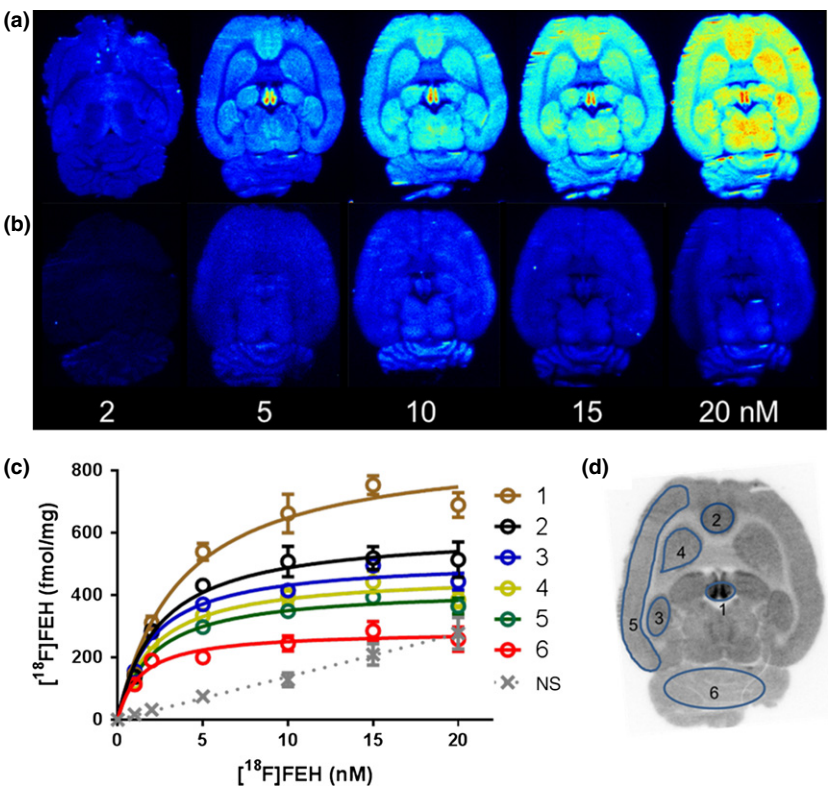

Fig. 1 (a and b) Autoradiograms of horizontal rat brain slices incubated with increasing concentrations of [18F]FEH showing total (a) and non-specific (b) binding. (c) Specific binding of [18F]FEH in various rat brain regions determined by quantitative *in vitro* autoradiography. ns: non-specific binding. Each data point represents the mean ± standard deviation (SD) from one representative experiment (N = 6). (d) Brain slice showing the defined region of interests (ROIs): (1) thalamus, (2) anterior cingulate cortex, (3) hippocampus, (4) striatum, (5) neocortex, and (6) cerebellum.

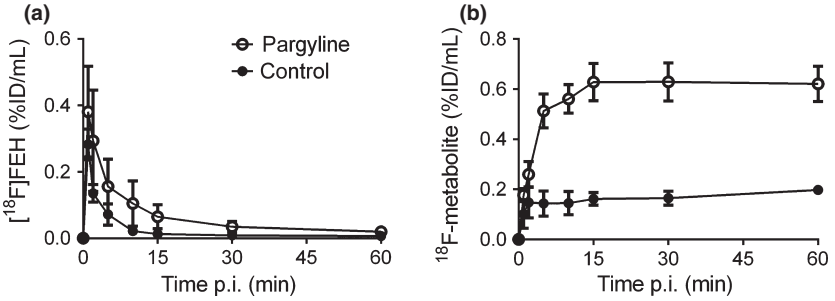

Fig. 2 Plasma concentrations of (a) intact [^{18}F]FEH and (b) its labeled metabolites as functions of circulation time post-injection (p.i.). Mean concentrations are presented the percentage injected dose per mL of plasma (%ID/mL) in the control and pargyline-treated groups. Each point represents the mean ± standard deviation from five animals.

Estimates of V_p, the apparent plasma volume, were approximately 3 mL/g in all rats. By 1TC analysis of regional volume of interest (VOI) data, the total distribution volume (V_T-1TC) ranged from 119 mL/g in cerebellum to 165 mL/g in thalamus of the control group, whereas V_D-1TC was uniformly close to 20 mL/g in the pargyline-treated group, indicating a BP_{ND} ranging from 4.2 in cerebellum to 7.2 in thalamus (Table 2, Fig. 5). Logan analysis of VOI data (Fig. 3c and d) gave similar results, but with some reduction in the range of BP_{ND} values between low and high binding regions. Although parametric Logan maps of V_T clearly depict the contrast between regions, and V_D maps depict the substantial displacement in the pargyline-treated groups (Fig. 4), calculations based on V_T-Logan and V_D-Logan in the VOIs did not capture the range of BP_{ND} by region (Table 2), apparently as a result of imprecision in the population mean estimates of V_D in the blocked condition, either by Logan or 1TC analysis.

The saturation binding study *in vivo* clearly depicted self-inhibition of binding in rats receiving [^{18}F]FEH of low specific activity (Fig. 5), especially when the injected mass exceeded 35 nmol, i.e., a specific activity < 0.5 MBq/μmol. Scatchard analysis gave *in vivo* K_D and B_{max} estimates (Fig. 5). In thalamus, striatum, and frontal cortex, K_D was close to 300 nM (ranging from 294 to 329 nM) and B_{max} close to 1600 pmol/g (ranging from 1580–1649 pmol/g), whereas in cerebellum K_D was 660 nM and B_{max} 2200 pmol/g.

Discussion

Ligands for monoamine oxidase may be enzyme substrates, suicide substrates, which form a covalent bond catalyzed by the enzyme itself, or ordinary reversible inhibitors of the enzyme. While the enzyme substrate [^{11}C]MPTP (^{11}C-N-methyl-4-phenyl-1,2,3,6-tetrahydropyridine) has been used to trace MAO-B activity in the living brain (Hartvig *et al.* 1986), only reversible and irreversible inhibitors have so far been tested for imaging MAO-A *in vivo*. A candidate SPECT (single photon emission computed tomography) radioligand for MAO-A imaging [^{125}I]moclobemide showed a BP_{ND} of approximately unity in the rat brain, as estimated from the tissue binding measured *ex vivo* at 1 h after i.v.

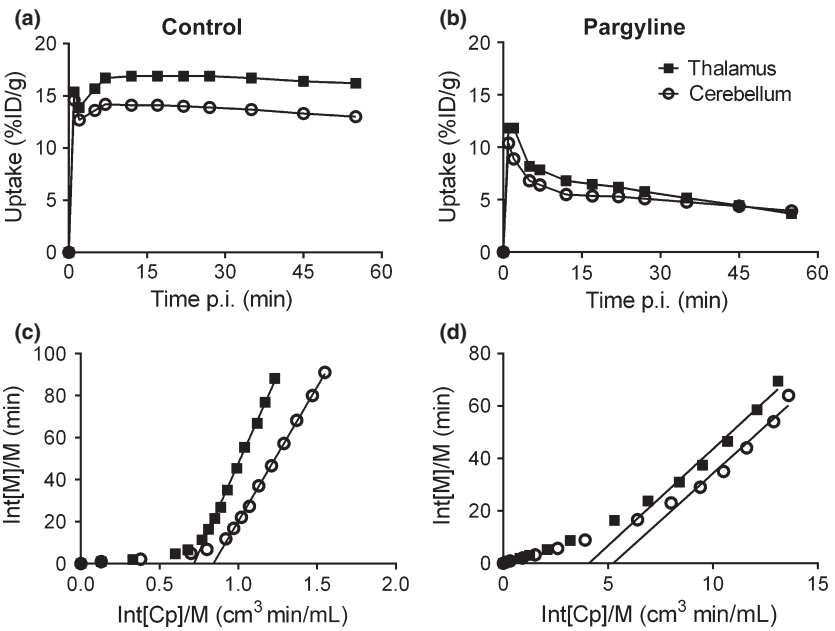

Fig. 3 Mean time–activity curves recorded for [^{18}F]FEH in thalamus and cerebellum in groups of five (a) control and (b) pargyline-treated rats, with normalization to the total injected tracer dose (%ID/g). The regression slopes of the late linear phases (solid lines) of representative Logan arterial input plots depict the tracer distribution volume in thalamus and cerebellum volumes of interest of an (c) control rat and (d) a pargyline-treated rat. Axis labels are expressed in terms of the radioactivity concentrations in brain (M) and plasma (Cp), and their integrals to time T (Int), according to the definition of the Logan plot.

Table 2 Mean kinetic results for the uptake of [18F]fluoroethyl-harmol ([18F]FEH) in four brain regions of living rats.

		Cerebellum	Cerebral cortex	Striatum	Thalamus
1-tissue compartment (1TC)					
K_1 (mL/g/min)	Control	1.40 ± 0.42	1.36 ± 0.42	1.44 ± 0.35	1.70 ± 0.40
	Pargyline	0.25 ± 0.15	0.30 ± 0.17	0.37 ± 0.21	0.36 ± 0.22
k_2 (per min)	Control	0.0122 ± 0.0043	0.0109 ± 0.0049	0.0098 ± 0.0033	0.0108 ± 0.0041
	Pargyline	0.014 ± 0.010	0.023 ± 0.014	0.030 ± 0.018	0.029 ± 0.018
Equilibrium distribution	Control (V_T-1TC)	119 ± 26	133 ± 28	155 ± 25	165 ± 30
volume (mL/g)	Pargyline (V_D-1TC)	23 ± 17	21 ± 20	20 ± 19	20 ± 19
BP_{ND} (VOI)		4.2 ± 1.1	5.3 ± 1.4	6.6 ± 1.3	7.2 ± 1.5
Logan					
VOI-wise equilibrium	Control (V_T-Logan)	119 ± 17	128 ± 28	146 ± 26	159 ± 28
distribution volume (mL/g)	Pargyline (V_D-Logan)	17 ± 12	17 ± 12	18 ± 13	17 ± 12
BP_{ND} (VOI-wise)		6.0 ± 1.0	6.5 ± 1.6	7.1 ± 1.4	8.4 ± 1.7
Voxel-wise equilibrium	Control (V_T-Logan)	143 ± 37	145 ± 36	150 ± 38	195 ± 40
distribution volume (mL/g)	Pargyline (V_D-Logan)	32 ± 31	33 ± 34	33 ± 33	39 ± 43
BP_{ND} (voxelwise)		3.5 ± 1.2	3.3 ± 1.0	4.5 ± 1.1	4.0 ± 1.0

Each result is the mean (± SD) of estimates in five control or five pargyline-treated animals. Results were calculated using a conventional 1-tissue compartment (1TC) model (K_1, k_2) for time–activity curves measured in the template VOIs (upper part of table), and the Logan arterial input linear estimation of distribution volumes (V_T-Logan and V_D-Logan) for time–activity curves in the VOIs, or the mean voxel-wise estimates from parametric maps. BP_{ND}, binding potential; VOI, volume of interest.

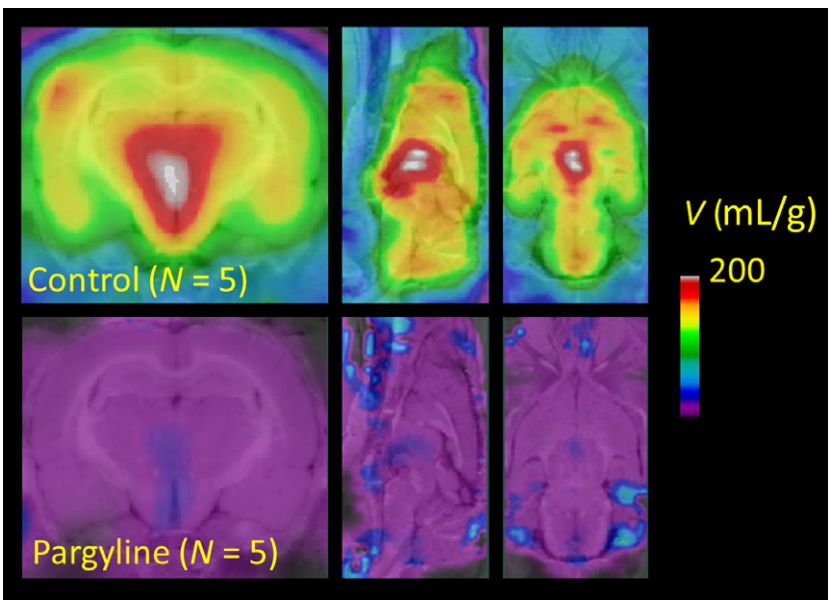

Fig. 4 Mean parametric maps of the total distribution volume (V_T) of [18F]FEH in brain of control rats (upper row), and the distribution volume (V_D) in a group of pargyline-treated rats (lower row), calculated voxel-wise by the Logan arterial input method. Parametric maps are projected upon an anatomic atlas for rat brain, depicted with gray scale. The equilibrium distribution volume (V; mL/g) is either the total distribution volume (V_T-Logan; upper row) or the non-specific distribution volume in the pargyline-blocked condition (V_D-Logan; lower row).

injection (Rafii *et al.* 1996). The irreversibly binding PET ligand [11C]clorgyline had binding in the white matter of human brain which was not entirely displaced by MAO-A inhibition (Fowler *et al.* 2001). Among the few reversibly binding PET ligands described for MAO-A are [11C]-ROMAO (1-(1-[11C]methyl-1*H*-pyrrol-2-yl)-2-phenyl-2-(1-pyrrolidinyl)ethanone), which had a BP_{ND} of unity in pig brain (Jensen *et al.* 2008), and [11C]befloxatone, which had a BP_{ND} of approximately five in baboon brain (Zanotti-Fregonara *et al.* 2013). The state of development of MAO ligands is the subject of a very recent review, which called for a concerted development of improved tracers (Fowler *et al.* 2015). The prototype reversible PET ligand for MAO-A is the β-carboline [11C]harmine (Bergström *et al.* 1997); in brain of living pigs, this tracer had a V_D close to 40 mL/g and a BP_{ND} as high as three (Jensen *et al.* 2006). Recent clinical research PET studies with [11C]harmine have revealed an association between MAO-A and depression (Chiuccariello *et al.* 2014), and have revealed dynamic changes in MAO-A availability in the brain of smokers

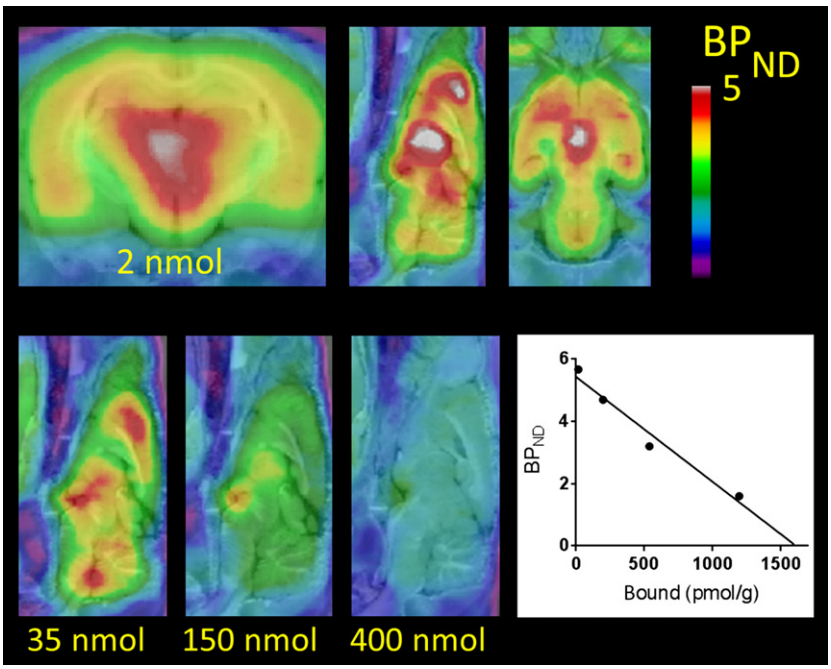

Fig. 5 Parametric maps for [^{18}F]FEH binding potential (BP_{ND}) as a function of specific activity. The upper row shows the mean results in the three planes for two rats receiving a total injected mass of 2 nmol, and the second row shows mean mid-sagittal slices for pairs of rats receiving higher injected masses. Maps are projected upon an anatomic atlas for rat brain. Using the estimated free concentration in cerebellum at 45–60 min post-injection, the insert shows the Scatchard graphical analysis for the case of thalamus, where each point represents the mean of two BP_{ND} determinations for a given specific activity, which differed by < 20%.

during withdrawal (Bacher *et al.* 2011). This renewed interest in MAO-A ligands for PET has led to improved and optimized [^{11}C]harmine radiosynthesis methods (Philippe *et al.* 2015). However, [^{11}C]harmine PET may suffer from two limitations; quantitation of the arterial input function is difficult because of the tracer`s rapid metabolism *in vivo*, and (more importantly), because of the 20 min physical half-life, it is only available to PET centers with a cyclotron-radiochemistry facility. These considerations have justified the further development of the harmine analogue [^{18}F]FEH (Cumming *et al.* 2015; Schieferstein *et al.* 2015).

[^{18}F]FEH autoradiography *in vitro* indicated a single saturable binding site in rat brain with affinity close to 2 nM, which is similar to the affinity reported for [^{11}C] harmine *in vitro* (Bergström *et al.* 1997) and to the IC_{50} reported previously for [^{18}F]FEH (Schieferstein *et al.* 2015). We found the MAO-A densities in rat brain to range from 337 pmol/g in cerebellum (the region of lowest abundance) to 836 pmol/g in the thalamus (the region of highest abundance). We see a focus of notably high MAO-A binding in the habenula, which is previously reported to contain 1.6 nmol/g MAO-A based on quantitative autoradiography with [^{14}C]clorgyline (Kondoh *et al.* 1994); only the locus coeruleus and interpeduncular nucleus had higher MAO-A binding in that study; we have earlier discerned [^{11}C]harmine binding in the locus coeruleus of living pigs (Jensen *et al.* 2006), but this was not evident in the present [^{18}F]FEH study, presumably because of greater effects of partial volume with μPET. The rank order and magnitude of present autoradiographic findings *in vitro* in cerebellum, striatum, and cerebral cortex match closely the results obtained earlier with [^{14}C]clorgyline, the irreversible ligand. Quantitative autoradiography with [^{18}F]FEH is favored by low non-specific binding, which did not exceed specific binding even at nearly saturating ligand concentrations (Fig. 1c).

Present and literature data afford the calculation of MAO-A homospecific activity, and the estimation of substrate concentrations in the living brain. The V_{max} for MAO-A in striatum homogenates is approximately 1 μmol/g/min with respect to dopamine, which had an affinity of about 200 μM (Cumming 2009); knowing the B_{max} in striatum (500 pmol/g), we can calculate the maximal catalysis rate (homospecific activity) to be 2000 dopamine per MAO-A enzyme per minute. The Michaelis–Menten constants *in vitro* predict a maximal dopamine turnover rate constant (V_{max}/K_m) of 5/min, predicting catabolism of dopamine in a matter of seconds. However, most striatal dopamine is normally confined to the vesicular compartment, such that the relative activity of MAO with respect to [^{3}H]dopamine formed in living striatum is only 0.01/min (Cumming *et al.* 1997). From this 500-fold difference (and neglecting contribution of MAO-B activity), we can calculate a dopamine metabolism rate of 2 nmol/g/min in living rat striatum, much less than the V_{max}. By substituting this rate (V_c) into the Michaelis–Menten equation, we can then estimate the concentration of free dopamine in the intracellular compartment to be 0.4 μM, which is very close to a direct measurement in the giant dopamine neuron of Planorbis (Chien *et al.* 1990). This result suggests that the concentration of cytoplasmic dopamine is not sufficient to cause a substantial displacement of reversibly binding MAO-A ligands *in vivo*, given the 200 μM affinity *in vitro*. This in turn predicts that modulation of [^{11}C]harmine binding reported in human PET studies with relatively mild pharmacological challenges (Sacher *et al.* 2012) cannot

readily be attributed to simple competition from endogenous substrates. On the other hand, complete MAO blockade with pargyline increased the dopamine concentration in whole rat brain by 50% without altering the concentration in the vesicular fraction (Buu and Lussier 1989); assuming a volume fraction for dopamine terminals of < 1%, this might predict a very substantial increase in the cytosolic dopamine concentration, perhaps sufficient to obtain some degree of occupancy of MAO-A, were it not already blocked by pargyline; we suppose that reserpine treatment, which degranulates vesicles but is not itself a potent MAO-A inhibitor, might transiently results in significant occupancy at MAO-A sites by cytosolic dopamine.

The metabolism of [18F]FEH in peripheral tissues is very rapid *in vivo*, as has been previously noted for [11C]harmine in pig (Jensen *et al.* 2006); only 11% of plasma radioactivity was untransformed parent at 10 min after [18F]FEH administration, and quantitation was difficult in the terminal (60 min) plasma extract. This result matches closely the findings of Schieferstein *et al.* (2015), who reported an attenuated metabolism for a deuterated derivative of [18F]FEH, albeit at the expense of reduced affinity for MAO-A *in vitro*. Despite the high plasma metabolite levels, nearly all of the radioactivity in brain extracts was untransformed parent. Although a rapidly declining arterial input function can present difficulties for quantitation of the cerebral tracer binding; nonetheless, we find a relative standard deviation of only about 20% for V_T, the parameter of main interest. Because of failure of initial attempts to measure the plasma free fraction (f_p), we could not systematically correct V_T for the individual f_p measurements, which were in the range of 36–54%, and were unaffected by pargyline treatment. This range of free fraction suggests that perhaps as much as half of the variance in V_T could be as a result of individual differences in serum albumin binding, although this must be moderated by the high initial clearance of [18F]FEH to brain. Until proven otherwise, it remains possible that individual differences in f_p may contribute to variance in V_T for [11C]harmine in human PET studies.

Regional estimates of the magnitude of V_D, i.e., distribution volume in the absence of specific binding, with a relative standard deviation of almost 100%, had considerably more variance than were the mean V_T estimates, discussed above. This variance seemed to be related to unusually rapid [18F]FEH metabolism rate constant (k_0) measured for two of the pargyline-treated animals. Based on methods reported by Müller Herde *et al.* (2015), the high distribution volume of [18F]FEH can be predicted from first principles; estimating the logP of FEH with ChemBioDraw to be 2.9, and knowing the compound to be neutral at physiological pH, we can estimate the distribution coefficient (D) to be $10^{2.9}$ or about 800. The magnitude of V_D (mL/g) for [18F]FEH is predicted as f_p*(0.1 × D + 1) = *circa* 35 mL/g, which is gratifyingly close to present findings in rat (20–30 mL/g, depending on method) and to findings for [11C]harmine in pig (Jensen *et al.* 2006) and human (Chiuccariello *et al.* 2014).

Unexpectedly, the AUC_{60} for [18F]FEH and likewise that for hydrophilic metabolite pool were 2.5-fold higher in the pargyline-treated group. This increase in plasma AUC was not associated with any reduction in the whole-body metabolism rate constant (k_0), whereas the fractional rate constant for clearance of the plasma metabolite pool (k_{-1}) was significantly higher in the pargyline group. This increased k_{-1} might suggest favoring of the [18F]FEH metabolism pathway to a more rapidly cleared metabolite after MAO-A blockade; indeed, Schieferstein *et al.* (2015) resolved two hydrophilic metabolites in their recent [18F]FEH study, whereas our chromatographic methods did not separate the metabolites. Pargyline is metabolized by de-alkylation (Baker *et al.* 1999), predicting competitive inhibition of specific cytochrome P450 enzymes, which might itself alter [18F]FEH levels in plasma, given that μM concentrations of β-carbolines inhibit P450 3A4 and 2D6 *in vitro* (Zhao *et al.* 2011). A more parsimonious explanation for the increased AUC may be that pargyline treatment occluded MAO-A sites in peripheral tissues, i.e., lungs, liver, and kidney (Fowler *et al.* 2004), resulting in greater plasma concentrations of [18F]FEH (and more metabolite formation) for a given radiotracer dose (Fig. 2a). Because of this phenomenon, our earlier use of a reference tissue method (the simplified reference tissue method) for calculating [18F]FEH BP_{ND} was invalid (Cumming *et al.* 2015), and indeed gave results approximately 2.5-fold lower than in this study as a result of uncorrected scaling of the arterial input function between control and pargyline-treated rats. Evidence for this phenomenon can also be seen in Fig. 5 of Schieferstein *et al.* (2015).

The non-physiologically high estimates of V_p (circa 3 mL/g) and K_1 (circa 1.4 mL/g/min) in the unblocked condition reflect the unfitness of the 1TC model for independently estimating this parameter for tracers of high permeability and high retention in the brain. Kinetic analysis of [18F]FEH uptake in brain of living rat in the pargyline-blocked condition indicated rapid unidirectional clearance from blood to brain. Despite under-sampling of the initial phase of the input function, the 1TC favors accurate estimation of K_1 (especially in the blocked condition) because of the rapidly declining arterial [18F]FEH concentrations, which imparts large weighting to the first time points. Assuming cerebral blood flow to be 0.5 mL/g/min, the global mean of the regional K_1 estimates (0.32 mL/g/min) suggest an extraction fraction of about 65%. We did not attempt a 2-tissue compartment model for the evaluation of rate constants (microparameters) for the reversible binding in brain, but instead focused on estimates of the steady-state distribution volumes. There was generally close agreement between V_D estimates obtained by 1TC analysis and by Logan`s linear regression method, although voxel-wise estimates tended to be higher than were the corresponding VOI-based estimates (Table 2), which may reflect bias in the

fitting of noisy data. As in our earlier [^{11}C]harmine pig study (Jensen *et al.* 2006), we calculated BP_{ND} relative to the V_D measured in the pargyline condition; no doubt we might have obtained more accurate estimates of individual BP_{ND}, had we measured V_D in each rat with MAO-A blockade, rather than using a separate group mean value. Regional BP_{ND} values in rat were only slightly higher than for [^{11}C]harmine in pig brain, suggesting a global scaling in the V_D and V_T estimates arising either from signal loss from small structures in the rat brain PET images or alternately from lower plasma protein binding (higher free fraction) in the case of the pig. The regional BP_{ND} values roughly match the rank order of regional MAO-A activity in homogenates from rat brain (Chalon *et al.* 1998), and also match the present findings by quantitative autoradiography. We note that the precision of BP_{ND} estimates was higher based upon compartmental analysis than by Logan analysis, perhaps as a result of exclusion of the initial data from the linear regression analysis.

Our attempt to measure saturation binding parameters for [^{18}F]FEH in the living brain was partially successful. Scatchard analysis did not clearly reveal regional heterogeneity in B_{max}, although the estimate was somewhat higher in cerebellum than in thalamus. The mean overall B_{max} *in vivo* was 2–6-fold higher than our regional estimates from autoradiography *in vitro*. Discrepancies between saturation binding parameters measured *in vivo* and *in vitro* are to be expected, due either to physiological or methodological factors. We have elsewhere noted fivefold higher B_{max} for the dopamine $D_{2/3}$ receptor ligand [^{11}C]raclopride by autoradiography (150 pmol/g) than is typical for PET-based estimates (30 pmol/g) (Cumming 2011), a discrepancy which we attributed to the presence of a receptor reserve unavailable for binding *in vivo*. The converse B_{max} discrepancy in this study might suggest that the MAO-A activity is lost during preparation of cryostat sections. However, an alternate possibility is suggested by the regional uniformity B_{max} *in vivo*, given a tendency for lower apparent K_D in the thalamus than in other brain regions. This observation suggests an unfavorable trade-off in the separate determination of B_{max} and K_D using present methods, where nonspecific binding was calculated by a most indirect procedure. We note that this study is the very first attempt to measure B_{max} for an enzyme *in vivo*, and propose that better estimates could be obtained if V_T and V_D were measured in the same individual animals through consecutive [^{18}F]FEH PET recordings in unblocked and blocked conditions. Present methodological limitations can hardly account for the 100-fold higher apparent K_D *in vivo*. A 10-fold discrepancy in the K_D of raclopride for dopamine receptors (2 nM *in vitro* vs. 20 nM *in vivo*) (Cumming 2011) is readily attributed to the free fraction for the radioligand in living brain, and to some competition from endogenous dopamine. Indeed, the high V_D of [^{18}F]FEH throughout the rat brain is consistent with a substantial partitioning of the ligand between lipid and aqueous phases, which likewise predicts a low free fraction in brain. Although calculations above may exclude the possibility of significant competition from endogenous dopamine, it may be that MAO-A in the living brain is constitutively inhibited, perhaps by β-carbolines derived from diet or second-hand smoke (Dixon Clarke and Ramsay 2011) or formed endogenously. A similar situation has been demonstrated in the case of MAO-B inhibition by the endogenous indole isatin (Crumeyrolle-Arias *et al.* 2004). We suppose that an extension of our method for estimating B_{max} and K_D in the living brain may allow the distinction of reversible and irreversible components of the MAO-A inhibition seen in smokers.

In summary, [^{18}F]FEH presents admirable properties for the detection of MAO-A by autoradiography *in vitro* and in PET studies of the living brain. The physical half-life of fluorine-18 may favor the use of this tracer as an alternative to [^{11}C]harmine. Nonetheless, the rapid plasma metabolism calls for particular attention to optimized analysis of the parent compound, and furthermore the plasma free fraction may contribute to variance in the apparent distribution volume. From a concordance of MAO-A enzyme activity and B_{max} measured *in vitro*, we calculate the homospecific activity of MAO-A and also estimate the concentration of dopamine in the cytosolic compartment of rat striatum. We present the first saturation binding study of an enzyme in the living brain, and find evidence for a very low tissue free fraction for [^{18}F]FEH.

Acknowledgments and conflict of interest disclosure

The authors thank Manuel Geisthoff for excellent assistance. The authors have no conflict of interest to be declared.

All experiments were conducted in compliance with the ARRIVE guidelines.

References

Bacher I., Houle S., Xu X. *et al.* (2011) Monoamine oxidase A binding in the prefrontal and anterior cingulate cortices during acute withdrawal from heavy cigarette smoking. *Arch. Gen. Psychiatry* **68**, 817–826.

Baker G. B., Urichuk L. J., McKenna K. F. and Kennedy S. H. (1999) Metabolism of monoamine oxidase inhibitors. *Cell. Mol. Neurobiol.* **19**, 411–426.

Bergström M., Westerberg G. and Langström B. (1997) ^{11}C-harmine as a tracer for monoamine oxidase A (MAO-A): in vitro and in vivo studies. *Nucl. Med. Biol.* **24**, 287–293.

Blom E., Karimi F., Eriksson O., Hall H. and Langström B. (2008) Synthesis and in vitro evaluation of ^{18}F-b-carboline alkaloids as PET ligands. *J. Labelled Compd. Radiopharmaceut.* **51**, 277–282.

Buu N. T. and Lussier C. (1989) Consequences of monoamine-oxidase inhibition - increased vesicular accumulation of dopamine and norepinephrine and increased metabolism by catechol-O-methyltransferase and phenolsulfotransferase. *Prog. Neuropsychopharmacol. Biol. Psychiatry* **13**, 563–568.

Chalon S., Delion-Vancassel S., Belzung C., Guilloteau D., Leguisquet A. M., Besnard J. C. and Durand G. (1998) Dietary fish oil affects monoaminergic neurotransmission and behavior in rats. *J. Nutr.* **128**, 2512–2519.

Chien J. B., Wallingford R. A. and Ewing A. G. (1990) Estimation of free dopamine in the cytoplasm of the giant dopamine cell of Planorbis corneus by voltammetry and capillary electrophoresis. *J. Neurochem.* **54**, 633–638.

Chiuccariello L., Houle S., Miler L. *et al.* (2014) Elevated monoamine oxidase A binding during major depressive episodes is associated with greater severity and reversed neurovegetative symptoms. *Neuropsychopharmacology* **39**, 973–980.

Crumeyrolle-Arias M., Tournaire M. C., Cane A., Launay J. M., Barritault D. and Medvedev A. (2004) Inhibition of brain mitochondrial monoamine oxidases by the endogenous compound 5-hydroxyoxindole. *Biochem. Pharmacol.* **67**, 977–979.

Cumming P. (2009) *Imaging Dopamine*. Cambridge University Press, Cambridge, United Kingdom.

Cumming P. (2011) Absolute abundances and affinity states of dopamine receptors in mammalian brain: a review. *Synapse* **65**, 892–909.

Cumming P., Brown E., Damsma G. and Fibiger H. (1992) Formation and Clearance of interstitial metabolites of dopamine and serotonin in the rat striatum - an in vivo microdialysis study. *J. Neurochem.* **59**, 1905–1914.

Cumming P., Ase A., Laliberte C., Kuwabara H. and Gjedde A. (1997) In vivo regulation of DOPA decarboxylase by dopamine receptors in rat brain. *J. Cereb. Blood Flow Metab.* **17**, 1254–1260.

Cumming P., Yokoi F., Chen A., Deep P., Dagher A., Reutens D., Kapczinski F., Wong D. F. and Gjedde A. (1999) Pharmacokinetics of radiotracers in human plasma during positron emission tomography. *Synapse* **34**, 124–134.

Cumming P., Maschauer S., Riss P. J., Tschammer N., Fehler S. K., Heinrich M. R., Kuwert T. and Prante O. (2014) Radiosynthesis and validation of ^{18}F-FP-CMT, a phenyltropane with superior properties for imaging the dopamine transporter in living brain. *J. Cereb. Blood Flow Metab.* **34**, 1148–1156.

Cumming P., Skaper D., Kuwert T., Maschauer S. and Prante O. (2015) Detection of monoamine oxidase a in brain of living rats with [^{18}F] fluoroethyl-harmol PET. *Synapse* **69**, 57–59.

Dixon Clarke S. E. and Ramsay R. R. (2011) Dietary inhibitors of monoamine oxidase A. *J. Neural. Transm.* **118**, 1031–1041.

Farde L., Hall H., Ehrin E. and Sedvall G. (1986) Quantitative analysis of D2 dopamine receptor binding in the living human brain by PET. *Science* **231**, 258–261.

la Fougere C., Boning G., Bartmann H. *et al.* (2010) Uptake and binding of the serotonin 5-HT1A antagonist [18F]-MPPF in brain of rats: effects of the novel P-glycoprotein inhibitor tariquidar. *NeuroImage* **49**, 1406–1415.

Fowler J. S., Logan J., Ding Y. S. *et al.* (2001) Non-MAO A binding of clorgyline in white matter in human brain. *J. Neurochem.* **79**, 1039–1046.

Fowler J. S., Logan J., Wang G. J. *et al.* (2004) Comparison of the binding of the irreversible monoamine oxidase tracers, [^{11}C]clorgyline and [^{11}C]L-deprenyl in brain and peripheral organs in humans. *Nucl. Med. Biol.* **31**, 313–319.

Fowler J. S., Logan J., Shumay E., Alia-Klein N., Wang G.-J. and Volkow N. D. (2015) Monoamine oxidase: radiotracer chemistry and human studies. *J. Labelled Compd. Radiopharmaceut.* **58**, 51–64.

Gryglewski G., Lanzenberger R., Kranz G. S. and Cumming P. (2014) Meta-analysis of molecular imaging of serotonin transporters in major depression. *J. Cereb. Blood Flow Metab.* **34**, 1096–1103.

Hartvig P., Larsson B. S., Lindberg B. S. *et al.* (1986) Influence of monoamine oxidase inhibitors and a dopamine uptake blocker on the distribution of 11C-N-methyl-4-phenyl-1,2,3,6-tetrahydropyridine, 11C-MPTP, in the head of the rhesus monkey. *Acta Neurol. Scand.* **74**, 10–16.

Innis R. B., Cunningham V. J., Delforge J. *et al.* (2007) Consensus nomenclature for in vivo imaging of reversibly binding radioligands. *J. Cereb. Blood Flow Metab.* **27**, 1533–1539.

Jahng J. W., Houpt T. A., Wessel T. C., Chen K., Shih J. C. and Joh T. H. (1997) Localization of monoamine oxidase A and B mRNA in the rat brain by in situ hybridization. *Synapse* **25**, 30–36.

Jensen S. B., Olsen A. K., Pedersen K. and Cumming P. (2006) Effect of monoamine oxidase inhibition on amphetamine-evoked changes in dopamine receptor availability in the living pig: a dual tracer PET study with [^{11}C]Harmine and [^{11}C]Raclopride. *Synapse* **59**, 427–434.

Jensen S. B., Di Santo R., Olsen A. K., Pedersen K., Costi R., Cirilli R. and Cumming P. (2008) Synthesis and cerebral uptake of 1-(1-[^{11}C]methyl-1H-pyrrol-2-yl)-2-phenyl-2-(1-pyrrolidinyl)ethanone, a novel tracer for positron emission tomography studies of monoamine oxidase type A. *J. Med. Chem.* **51**, 1617–1622.

Kondoh Y., Murakami M., Yin W., Mizusawa S., Nakamichi H. and Nagata K. (1994) Quantitative distribution of rat brain monoamine oxidase A by [^{14}C]clorgyline autoradiography. *Exp. Brain Res.* **99**, 375–378.

McKenna D. J., Towers G. H. and Abbott F. (1984) Monoamine oxidase inhibitors in South American hallucinogenic plants: tryptamine and beta-carboline constituents of ayahuasca. *J. Ethnopharmacol.* **10**, 195–223.

Müller Herde A., Keller C., Milicevic Sephton S., Mu L., Schibli R., Ametamey S. M. and Kramer S. D. (2015) Quantitative positron emission tomography of mGluR5 in rat brain with [^{18}F]PSS232 at minimal invasiveness and reduced model complexity. *J. Neurochem.* **133**, 330–342.

Philippe C., Zeilinger M., Mitterhauser M., Dumanic M., Lanzenberger R., Hacker M. and Wadsak W. (2015) Parameter evaluation and fully-automated radiosynthesis of [^{11}C]harmine for imaging of MAO-A for clinical trials. *Appl. Radiat. Isot.* **97**, 182–187.

Rafii H., Chalon S., Ombetta J. E., Frangin Y., Pourcelot L., Besnard J. C., Bodard S. and Guilloteau D. (1996) An iodinated derivative of moclobemide as potential radioligand for brain MAO-A exploration. *Life Sci.* **58**, 1159–1169.

Sacher J., Rabiner E. A., Clark M. *et al.* (2012) Dynamic, adaptive changes in MAO-A binding after alterations in substrate availability: an in vivo [(11)C]-harmine positron emission tomography study. *J. Cereb. Blood Flow Metab.* **32**, 443–446.

Schieferstein H., Piel M., Bausbacher N. and Roesch F. (2012) In vivo evaluation of pegylated [^{18}F]harmine derivatives: selective reversible MAO-A inhibitors. *J. Nucl. Med.* **53**, 1612.

Schieferstein H., Piel M., Beyerlein F., Luddens H., Bausbacher N., Buchholz H. G., Ross T. L. and Rosch F. (2015) Selective binding to monoamine oxidase A: in vitro and in vivo evaluation of F-18-labeled beta-carboline derivatives. *Bioorg. Med. Chem.* **23**, 612–623.

Zanotti-Fregonara P., Leroy C., Roumenov D., Trichard C., Martinot J. L. and Bottlaender M. (2013) Kinetic analysis of [^{11}C]befloxatone in the human brain, a selective radioligand to image monoamine oxidase A. *EJNMMI Res.* **3**, 78.

Zhao T., He Y. Q., Wang J., Ding K. M., Wang C. H. and Wang Z. T. (2011) Inhibition of human cytochrome P450 enzymes 3A4 and 2D6 by beta-carboline alkaloids, harmine derivatives. *Phytother. Res.* **25**, 1671–1677.

Zhou Y., Huang S. C., Bergsneider M. and Wong D. F. (2002) Improved parametric image generation using spatial-temporal analysis of dynamic PET studies. *NeuroImage* **15**, 697–707.